Inference with finite time series: Observing the gravitational Universe through windows

Colm Talbot,[1, a] Eric Thrane,[2, 3] Sylvia Biscoveanu,[4] and Rory Smith[2, 3]

[1]*LIGO Laboratory, California Institute of Technology, Pasadena, CA 91125, USA*
[2]*School of Physics and Astronomy, Monash University, VIC 3800, Australia*
[3]*OzGrav: The ARC Centre of Excellence for Gravitational-Wave Discovery, Clayton, VIC 3800, Australia*
[4]*LIGO, Massachusetts Institute of Technology, Cambridge, Massachusetts 02139, USA*

Time series analysis is ubiquitous in many fields of science including gravitational-wave astronomy, where strain time series are analyzed to infer the nature of gravitational-wave sources, e.g., black holes and neutron stars. It is common in gravitational-wave transient studies to apply a tapered window function to reduce the effects of spectral artifacts from the sharp edges of data segments. We show that the conventional analysis of tapered data fails to take into account covariance between frequency bins, which arises for all finite time series—no matter the choice of window function. We discuss the origin of this covariance and show that as the number of gravitational-wave detections grows, and as we gain access to more high signal-to-noise ratio events, this covariance will become a non-negligible source of systematic error. We derive a framework that models the correlation induced by the window function and demonstrate this solution using both data from the first LIGO–Virgo transient catalog and simulated Gaussian noise.

I. INTRODUCTION

Time-series analysis underpins recent advances in gravitational-wave astronomy. The vast majority of gravitational-wave data analysis relies on windowing, a procedure that multiplies the time-domain data segment by a window function that tapers off at the beginning and end of the segment. Analysts apply tapered windows to mitigate two effects: (1) spectral artifacts arising from the Fourier transform of the data segment edges (Gibbs phenomena) and (2) correlations between neighboring frequency bins. Choosing a suitable window requires balancing various considerations including the spectral leakage from lines, effectiveness mitigating the Gibbs phenomenon, and the loss of signal. For a systematic study of the properties of different windows, we refer the reader to the classic paper by Harris [1]. Once the data are windowed, they are typically analyzed in the frequency domain where the noise is described by a power spectral density (PSD), and it is assumed that each frequency bin is statistically independent. However, this assumption is not true for a finite stretch of a longer noise process.

The assumptions underpinning the Whittle approximation have been thoroughly studied and many refinements have been proposed (e.g., [2–6]). In this paper, we derive from first principles a formalism which accounts for the correlations between neighboring frequencies introduced by the window function applied to obtain finite time series. We show how correlations between frequency bins arise from the fact that quasi-stationary Gaussian noise processes are fundamentally described in the frequency domain by continuous functions, which imply *infinite-duration* time series. We derive a simple expression for the "finite-duration" covariance matrix, which encodes the correlations naturally present in all finite time series and identify our result as a specific basis for a Karhunen-Loève transformation (KLT) (see, e.g., [7]). We show that there are practical applications where the current conventional approach of windowing data incurs systematic errors, which though small, produce invalid inferences when data are combined in large sets or when we analyze gravitational-wave events with high signal-to-noise ratio (SNR).

The remainder of this paper is organized as follows. In Section II, we present the formalism underlying our framework. We derive the finite-duration covariance matrix for the analysis of finite time series. In Section III, we perform a demonstration, applying our method to the binary black hole merger events, GW150914 [8], GW170814 [9], and GW190521 [10] and contrast with results neglecting covariances. We show how the current conventional windowing procedure can lead to faulty inferences when many gravitational-wave measurements are combined. While our demonstration uses data from gravitational-wave astronomy, the framework we put forward is broadly applicable to all time-domain analysis. We show that the problem is fixed by using the finite-duration covariance matrix. We provide closing thoughts in Section IV.

II. FORMALISM

In this section, we derive a likelihood that enables us to analyze time-series data characterized by stationary, Gaussian noise in a way that correctly takes into account covariance between neighboring frequency bins that arises for all finite time series.

[a] ctalbot@caltech.edu

A. Basic notation

We consider time-series data $d(t)$ consisting of signal $s(t)$ and noise $n(t)$

$$d(t) = s(t) + n(t). \tag{1}$$

In gravitational-wave observatories like LIGO [11] and Virgo [12], $n(t)$ is a time series of dimensionless strain (change in length per unit length). Transient gravitational-wave signals from merging binaries are characterized by comparing the data to gravitational waveform templates $h(t)$.

B. Continuous, infinite-duration noise

To start, we focus on noise in the absence of signals. The noise can be expressed in the frequency domain as

$$\tilde{n}(f) = \int_{-\infty}^{\infty} dt\, e^{-2\pi i f t} n(t). \tag{2}$$

The noise is best described as continuous because it is defined for an arbitrary choice of frequency: with a sufficiently long measurement, it is possible *in principle* to achieve sufficient resolution to measure $\tilde{n}(f)$ for any value of f.

If we assume the noise is Gaussian, the likelihood of observing a specific noise realization is characterized by a covariance matrix

$$\mathcal{C}_{\mu\nu} = \frac{1}{2} \left\langle \tilde{n}(f_\mu) \tilde{n}^*(f_\nu) \right\rangle \tag{3}$$

the diagonal of which is equal to the noise PSD $\mathcal{S}$

$$\mathcal{S}_\mu = \text{diag}\left(\mathcal{C}_{\mu\nu}\right). \tag{4}$$

We refer to $\mathcal{C}_{\mu\nu}$ as the "infinite-duration" covariance matrix. It is defined *continuously* for arbitrary values of f_μ and f_ν and, in the time domain, it is defined for all times: $(-\infty, +\infty)$. Throughout, repeated indices are summed over unless otherwise specified (e.g., Eq. 4). In the next subsection, we contrast $\mathcal{C}_{\mu\nu}$ (calligraphic script and Greek indices) with the finite-duration covariance matrix, denoted C_{ij} (no calligraphic script and Roman indices), which is defined only for discrete frequency bins f_i and f_j (or equivalently, for a finite duration). If we further assume that the noise is stationary (the PSD does not vary in time), $\mathcal{C}_{\mu\nu}$ is diagonal.

C. Non-continuous, finite-duration noise

In practice, we only consider finite stretches of data. In this subsection, we derive the properties of finite stretches of continuous noise. Let us consider data measured with sampling rate f_s over data segment duration T. There are

$$N = f_s T, \tag{5}$$

independent measurements. We assume that the noise has no content above half the sampling rate and so we can probe every frequency without aliasing. In practice, applying an aggressive low-pass filter removes this high frequency content.

These data can be represented either in the time-domain as a real N-component time series with spacing $1/f_s$ or in the frequency domain as a complex frequency series $\tilde{d}_i$ with $-f_s/2 \leq f \leq f_s/2$ with spacing $1/T$ where the endpoints and zero-frequency component are required to be real. These two domains are related via the discrete Fourier transform [13]

$$\tilde{d}'_k = \frac{1}{f_s} \sum_{j=0}^{N-1} d'_j e^{-2\pi i j k/N}. \tag{6}$$

The frequency-domain covariance matrix for finite-duration, non-continuous noise is:

$$C_{ij} = \frac{1}{2} \left\langle \tilde{d}'_i \tilde{d}^{*\prime}_j \right\rangle. \tag{7}$$

Here, the angled brackets denote ensemble averages over noise realizations. The widely-used Whittle approximation assumes that data at each of the analyzed frequencies are independent, i.e., C_{ij} is a diagonal matrix. This is generally a good approximation. However, as we show in this work, the assumption of independence is not strictly valid when analyzing a finite stretch of data, especially when using a tapered window.

We begin by defining our window function w, which describes how we measure some segment of noise from what is, in theory, an infinite-duration noise process:

$$\tilde{d}'_k = \frac{1}{f_s} \sum_{\psi=-\infty}^{\infty} d_\psi w_\psi e^{-2\pi i \psi k/N} \tag{8}$$

$$= \frac{1}{f_s} \sum_{j=0}^{N} d_j w_j e^{-2\pi i j k/N} \tag{9}$$

$$= (\tilde{d} * \tilde{w})_k. \tag{10}$$

Here, w_j is a time-domain window function and the frequency-domain noise is now the convolution of the original frequency-domain noise with the Fourier transformed window function. The prime denotes quantities associated with the windowed data.

We stress that this window function is always present in gravitational-wave data analysis problems and is defined for all times, not just the analysis segment. It is often ignored when it is a top hat function, i.e.,

$$w_\psi = \begin{cases} 1 & 0 \leq \psi < N \\ 0 & \text{else} \end{cases}. \tag{11}$$

The most commonly used window function in parameter estimation for compact binary coalescences is the Tukey window

$$w_\psi(\alpha) = \begin{cases} \frac{1}{2}\left[1-\cos\left(\frac{2\pi\psi}{\alpha N}\right)\right] & 0<\psi<\frac{\alpha N}{2} \\ 1 & \frac{\alpha N}{2}\le\psi\le N-\frac{\alpha N}{2} \\ \frac{1}{2}\left[1-\cos\left(\frac{2\pi(N-\psi)}{\alpha N}\right)\right] & N-\frac{\alpha N}{2}<\psi<N \\ 0 & \text{else} \end{cases}. \tag{12}$$

Common limiting cases of the Tukey window are the rectangular window ($\alpha = 0$) and the Hann window ($\alpha = 1$). Throughout this work, we use Tukey windows with $\alpha = 0.1$ unless otherwise specified, although the formalism described here holds for arbitrary window functions.

Since convolution is a linear operation, we can express the windowed frequency-domain data using standard linear algebra notation

$$\tilde{d}'_k = \tilde{W}_{k\mu}\tilde{d}_\mu, \tag{13}$$

where repeated indices denote summation. Here, $\tilde{W}_{k\mu}$ is a non-square subset of the circulant matrix

$$\tilde{W}_{\mu\nu} = \tilde{w}_{\mu-\nu} \tag{14}$$

that projects infinite-duration noise with frequency resolution $\delta f \to 0$ to finite duration data with frequency resolution $1/T$. Here, $\tilde{w}$ is the discrete fourier transform of the time-domain window function.

We can now write the covariance matrix for a finite-duration data stream with an arbitrary window function in terms of the frequency-domain covariance matrix of the infinite-duration process and the window function using Eq. 7 and Eq. 13

$$C_{ij} = \frac{1}{2}\left\langle \tilde{W}_{i\mu}\tilde{W}^*_{j\nu}\tilde{d}_\mu\tilde{d}^*_\nu\right\rangle \tag{15}$$

$$= \frac{1}{2}\tilde{W}_{i\mu}\tilde{W}^*_{j\nu}\left\langle\tilde{d}_\mu\tilde{d}^*_\nu\right\rangle$$

$$= \tilde{W}_{i\mu}\tilde{W}^*_{j\nu}\mathcal{C}_{\mu\nu}. \tag{16}$$

If the underlying data are Gaussian and stationary, $\mathcal{C}_{\mu\nu}$ is diagonal and the finite-duration covariance matrix only depends on the window function and the infinite-duration PSD. While we initially defined the Roman indices as covering frequencies from $[-f_s/2, f_s/2]$, in practice we analyze a narrower (positive) frequency range from $[f_{\rm min}, f_{\rm max}]$. In this work we will set $f_{\rm min} = 20$ Hz, $f_{\rm max} = 800$ Hz; this omits data are affected by the bandpass filter we apply. From here, Roman indices will refer to this frequency range only.

Formally, one must carry out matrix products over the infinite axes denoted by Greek indices to obtain the finite-duration covariance matrix in Eq. 16. In practice, however, via numerical experiment we find that infinite-duration matrices can be adequately approximated using a frequency resolution 16 times that of the analysis segment. In other words, when analysing a 4 s data segment (frequency resolution = 0.25 Hz), we may model infinite-duration noise with a 1/64 Hz (or higher-resolution) noise model. The resolution of the noise model can be tuned to achieve the necessary precision for a given problem.

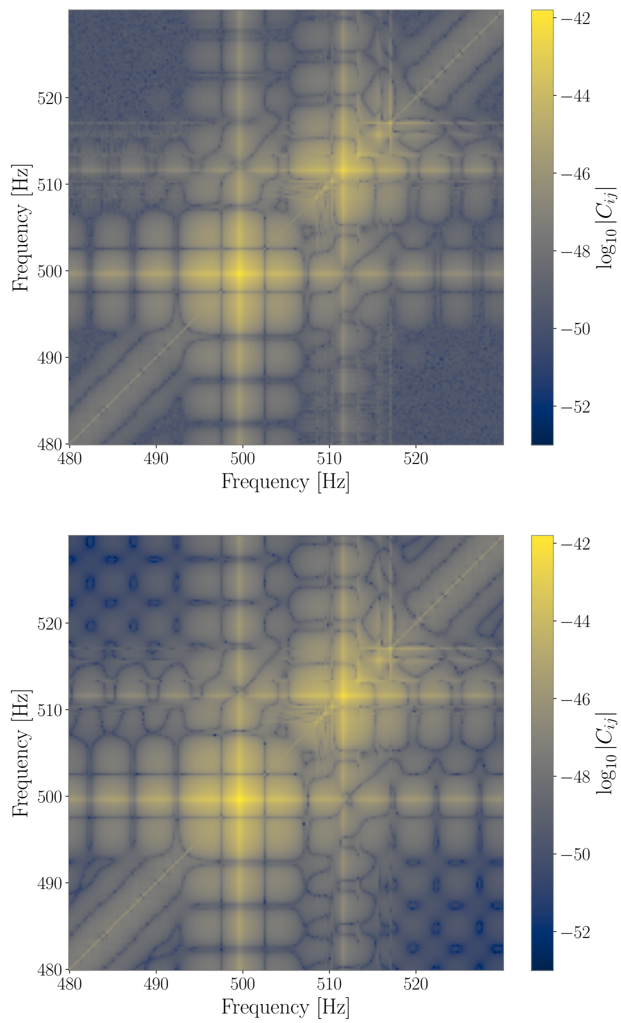

FIG. 1. The estimated (top) and analytic (bottom) covariance matrix for simulated noise using a noise power spectral density estimated from LIGO Livingston data around the time of the binary black hole merger GW170814. The color bar indicates $\log_{10}$ power spectral density in units of strain^{2}Hz^{-1}. The estimate is obtained using ~ 3 months of simulated data. The off-diagonal behaviour agrees well with the analytic expression. The window used is a Tukey window with $\alpha = 0.1$.

In Fig. 1 we show the empirical finite-duration covariance matrix in the neighborhood of the diagonal—obtained by averaging ~ 3 months of simulated Gaussian noise broken into 10^{21} 4 s segments and using a Tukey window with $\alpha = 0.1$ (Eq. 7) (top panel)—compared with the exact finite-duration covariance matrix obtained with our analytic expressions (Eq. 16) (bottom panel). The underlying PSD ($\mathcal{S}_\mu$) is estimated using data from the LIGO Livingston interferometer at the time of the binary black hole merger GW170814 with a resolution of 1/128 Hz. The two panels agree well, demonstrating the correctness of this formalism. However, the averaging estimate converges unacceptably slowly for practical use, and so our analytic expression is essential for practical applications.

We are interested in the inverse of the covariance matrix C^{-1}_{ij}. We discuss the issue of inverting this matrix in Sec. II E. We also emphasize that the finite-duration PSD (the leading diagonal of C_{ij}) $S_i \neq \mathcal{S}_i$, i.e., the finite-duration PSD is not the infinite-duration evaluated at the desired frequencies. Additional technical details about this formalism are provided in the Appendix. In Appendix A, we discuss how our formalism is related to "coarse-graining" procedures used for PSD estimation (e.g., [14]). In Appendix B and Algorithm 1, we describe in detail how we approximate $\mathcal{C}_{\mu\nu}$ and C_{ij} from real data.

D. Covariance from spectral lines

From Fig. 1, we see that windowing produces off-diagonal elements in the finite-duration covariance matrix in general. In this subsection, we illustrate how this covariance is compounded by sharp spectral features. The relationship between the choice of window and spectral leakage from sharp spectral features is well known in signal processing; see, e.g., [1]. In gravitational-wave detectors, there are a number of such features commonly referred to as "lines" [15]. The leading-order correction from the off-diagonal components of the covariance matrix are most clearly seen using the following metric:

$$\max_{i\neq j}\left|\frac{C_{ij}}{S_j}\right|. \tag{17}$$

In Fig. 2, we show this quantity for the PSDs used in our analysis of the gravitational-wave signal, GW170814 [9] (Sec. III A), which was observed in 2017 by the Advanced LIGO [11] and Virgo [12] observatories. For the two LIGO observatories [11], the magnitude of the off-diagonal terms is approximately constant throughout the observing band with exceptions for the known lines. The "violin modes" for the Livingston interferometer (~ 500 Hz) are significantly larger than for the Hanford interferometer and the the contamination near the lines is larger and more broadband. Given this behavior, one might think that we can neglect the impact of the off-diagonal terms if we remove from the analysis the frequency bins in the neighborhood of the lines. However, for the Virgo observatory [12], we see that the average correction is much larger across most of the band and is frequently $> 20\%$. This can be attributed to the Virgo PSD being less smoothly varying. A cut based on frequencies with unacceptably large contamination would remove most of the observing band. However, data analysis with the finite-duration covariance matrix can be used to take into account covariance in Virgo noise.

E. Regularized inversion

Having characterized the covariance between frequency bins due to windows, we turn to the inversion of the covariance matrix required to evaluate the likelihood function. Since tapered window functions go to zero at the edges by construction, the covariance matrix is not invertible [16]. To deal with this issue, we perform a regularized inversion using a singular value decomposition (SVD) and discard the smallest eigenvalues. The SVD of a Hermitian matrix can be written as

$$C_{ij} = U_{ik}\Lambda_{kl}U^{-1}_{lj}. \tag{18}$$

Here, $\Lambda_{kl} = \delta_{kl}\lambda_k$ (no summation) is a diagonal matrix with the eigenvalues λ_k on the leading diagonal. Regularization simply involves removing eigenmodes corresponding to small eigenvalues. In practice, this is done by setting the eigenvalue to ∞

$$\bar{\lambda}_i = \begin{cases}\lambda_i & i \leq \epsilon N\\ \infty & i > \epsilon N\end{cases} \tag{19}$$

where a fraction ϵ of the N eigenmodes are retained. The regularized matrix and its inverse are

$$\bar{C}_{ij} = U_{ik}\bar{\Lambda}_{kl}U^{-1}_{lj} \tag{20}$$

$$\bar{C}^{-1}_{ij} = U_{ik}\bar{\Lambda}^{-1}_{kl}U^{-1}_{lj}. \tag{21}$$

In Fig. 3, we show the eigenvalues in decreasing order for the covariance matrix estimated at the time of GW170814. We identify three regimes in the eigenvalue spectrum:

1. Large eigenvalues with a steep slope at low eigenmode number. These predominantly correspond to frequencies where C_{ij} is large, e.g., near spectral lines and at low frequencies.

2. A slowly varying region encompassing the majority of the eigenvalues. This corresponds to the remainder of the frequencies where the PSD is smoothly varying.

3. A rapid drop to the smallest eigenvalues. This is a characteristic feature of ill-conditioned matrices and is the region we should remove when regularizing.

We determine the fraction of eigenvalues to discard by considering the power loss from the window function. The amount of information lost by the window is related to the time-averaged square of the window function. The effective number of independent time samples is

$$N_{\text{eff}} = N\overline{w^2} = N\int dt\, w^2(t) \approx \sum_{i=0}^{N-1} w_i^2. \tag{22}$$

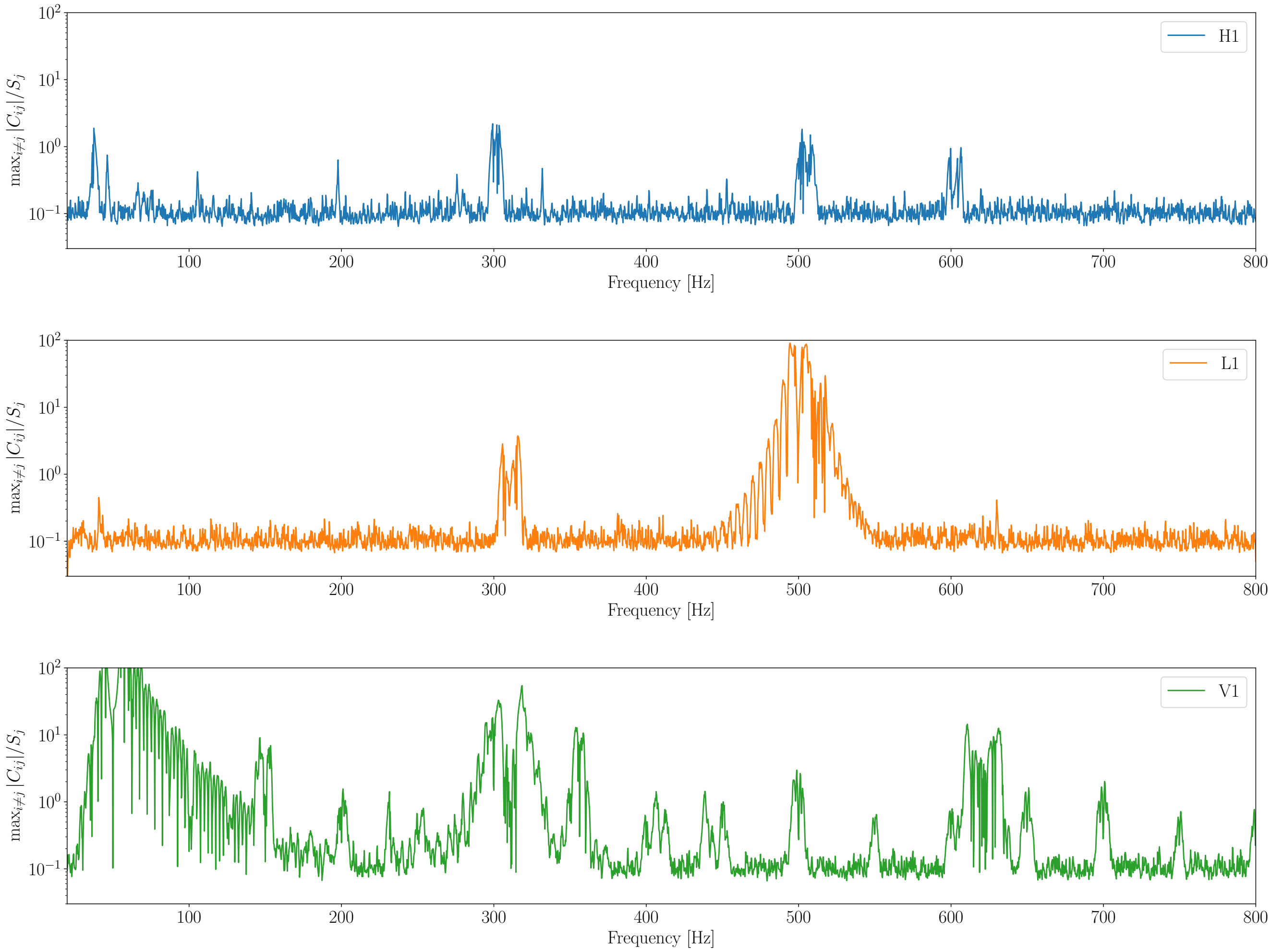

FIG. 2. Maximum contamination per frequency bin (Eq. 17) for PSDs estimated near the time of binary black hole merger GW170814 [9]. We see two competing effects. First, there is broadband contamination at $\sim 10\%$ when the PSD is slowly varying. The magnitude of this contamination rises with increasing Tukey α. There is also large contamination near instrumental lines due to spectral leakage.

We choose the fraction of eigenvalues to remove based on the window function

$$\epsilon = 1 - \frac{N_{\text{eff}}}{N} = 1 - \overline{w^2}. \tag{23}$$

The vertical lines are at N_{eff} and show the number of modes we omit to account for the information loss due to the tapered window, we note that this matches well the transition to the badly bahaved modes.

F. Finite-duration likelihood

We can now write our final result, the regularized likelihood with a finite-duration covariance matrix:

$$\bar{\mathcal{L}}(\tilde{d}|\theta, \bar{C}) = \frac{2}{T \det \bar{C}} \exp\left[-\frac{2}{T}\left\langle \tilde{d} - \tilde{h}, \tilde{d} - \tilde{h}\right\rangle_{\bar{C}}\right]. \tag{24}$$

where $\det \bar{C}$ is the determinant of the finite-duration noise covariance matrix, $\tilde{h}$ is a template for the signal and the inner product is defined as

$$\langle \tilde{x}, \tilde{x}\rangle_{\bar{C}} = \tilde{x}_i \bar{C}^{-1}_{ij} \tilde{x}^*_j. \tag{25}$$

As the exponent in the likelihood can still be written as weighted inner products between data and template, we can analytically marginalize over extrinsic parameters in the same way as for the diagonal likelihood [17].

G. Relation to the Karhunen-Loève transform

The Karhunen-Loève theorem states that for any stochastic process there exists a basis in which the noise covariance matrix is diagonal and the transformation into this basis is referred to as the KLT. For a colored stationary Gaussian process that is periodic with period T, this

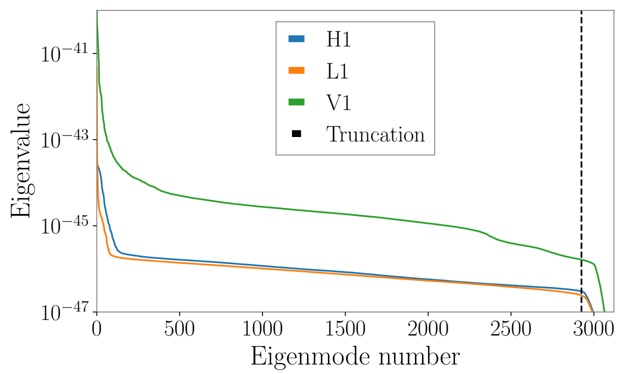

FIG. 3. Eigenvalues of an estimated noise power covariance matrix for data close to GW170814 for a Tukey window with $\alpha = 0.1$. The vertical lines denote the points after which we discard the eigenmodes as determined by the window information loss. The large eigenvalues correspond to spectral lines and the low-frequency seismic wall; the slowly varying region corresponds to the smoothly varying observing band. This well-approximates the turnover after which the eigenvalues rapidly decline due to information loss from windowing.

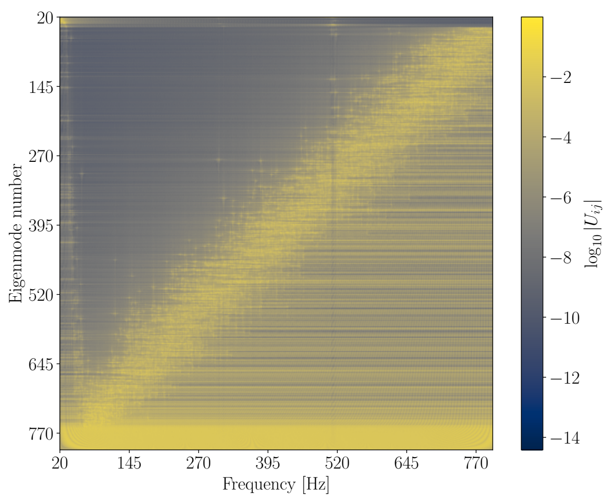

FIG. 4. Eigenmodes for the covariance matrix estimated from data from the LIGO Livingston interferometer close to GW170814. This matrix encodes the correlations between physical frequencies. The horizontal axis corresponds to the physical frequencies, while the vertical axis is the order of decreasing eigenvalue. The bottom-most eigenmodes are the ones that are discarded. These eigenmodes are associated with very broadband frequency content.

basis is the discrete Fourier transform with spacing $1/T$ Hz. The Whittle likelihood approximation specifically assumes that this basis also diagonalizes the covariance matrix for a subset of a longer Gaussian process that is not periodic with period T. As we have demonstrated, the covariance matrix in the Fourier basis is not diagonal in this case.

We note that the KLT is closely related to the SVD and therefore identify that the basis for the KLT of a finite subset of a longer Gaussian process is the basis found in Section II E. This provides a second, equivalent, interpretation of the inner product in Eq. 25

$$\langle \tilde{x}, \tilde{x} \rangle_{\bar{C}} = \tilde{x}_i U_{ik} \bar{\Lambda}^{-1}_{kl} U^{-1}_{lj} = \sum_i \frac{|\bar{x}_i|^2}{\bar{\lambda}_i}. \tag{26}$$

Where we have defined $\bar{x}_i \equiv \tilde{x}_i U_{ik}$. The likelihood is now

$$\ln \mathcal{L} = -\sum_i \left[\frac{|\bar{d}_i - \bar{h}_i|^2}{\lambda_i} + \ln(\lambda_i) \right] + \text{const}. \tag{27}$$

We identify that this has the usual form of the likelihood except that all of the quantities are described in the eigenbasis of the KLT, rather than the Fourier basis.

III. DEMONSTRATION

To demonstrate our formalism we perform two tests. First, we analyze three binary black hole mergers to demonstrate that the effect of the off-diagonal corrections is small but noticeable for confidently detected signals. Second, we demonstrate that although this effect produces a minor correction to modest-SNR events, neglecting the impact of off-diagonal terms in the noise covariance matrix biases precision estimates, such as evidence calculations required for searches for a population of weak, sub-threshold signals as in [18].

A. Single events

We compare the posterior distributions obtained using both the conventional and finite-duration covariance matrices for three of the observed binary black hole mergers GW150914 [8], GW170814 [9], and GW190521 [10]. We choose these as they are relatively high-mass systems (with detector frame primary and secondary masses of $m_1 \approx m_2 \approx 30 - 40 M_\odot$ for GW150914 and GW170814 and $m_1 \approx m_2 \approx 150 M_\odot$ for GW190521) for which we expect the tapered window to have a comparatively large impact on the data. They also span a large range in time, with one event from each of the first three observing runs of the advanced detector network, leading to significantly different PSDs.

For each event, we analyze 4 s of data centered at the trigger time for event and estimate the PSD using a 512 s stretch of data ending 2 s before the trigger. We apply a band-pass filter between 16 Hz and 1024 Hz and resample the data to a new Nyquist frequency of 2048 Hz using `GWpy` [19] to mitigate spectral leakage from low and high frequencies. We use a Tukey window with $\alpha = 0.1$ for the analysis segment. The details of the covariance matrix calculation are described in Algorithm 1. We employ the `IMRPhenomXPHM` waveform approximant [20–22] in the

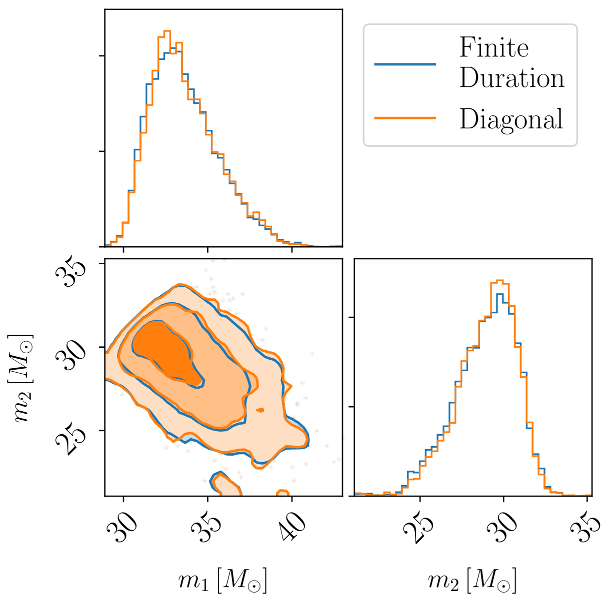

FIG. 5. Intrinsic parameters for the binary black hole merger GW150914 [8] using the diagonal likelihood (blue) and our new finite-duration likelihood (orange). The primary and secondary mass (m_1, m_2) refer respectively to the more-massive and less-massive component masses. Including covariance between neighbouring bins has no observable impact on the inferred posterior.

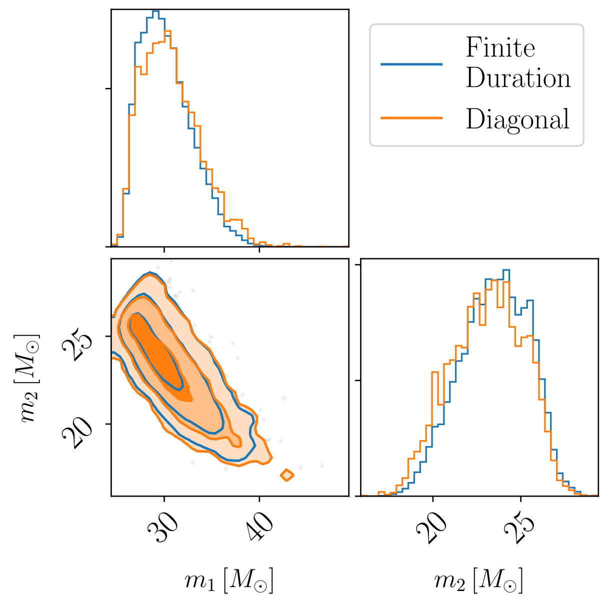

FIG. 6. Intrinsic parameters for the binary black hole merger GW170814 [9] using the diagonal likelihood (blue) and our new finite-duration likelihood (orange). The primary and secondary mass (m_1, m_2) refer respectively to the more-massive and less-massive component masses. Including covariance between neighbouring frequency bins slightly shifts the inferred posterior distribution for the mass ratio.

frequency range $20 - 800\,\mathrm{Hz}$; for GW190521 we set the upper frequency limit as $300\,\mathrm{Hz}$. We neglect the impact of calibration uncertainty or uncertainty in our estimate of the PSD. For GW150914, we analyze data from the two LIGO interferometers, for the other two events, we analye data from the two LIGO interferometers and Advanced Virgo.

We show the posterior distribution for four of the intrinsic binary parameters for the diagonal likelihood (blue) and finite-duration likelihood (orange) for GW150194 GW170814, GW190521 in Figs. 5, 6, and 7 respectively. The primary and secondary mass refer respectively to the more-massive and less-massive black-hole masses. The largest difference we see is in the component masses for GW170814, primarily driven by a change in the inferred mass ratio. There is no visible difference between the posteriors for the other events. The change in the posterior distributions is at a similar level to the changes due to marginalizing over uncertainty in the detector calibration [23, 24] or PSD estimate [6, 25, 26], but less than the difference due to using different PSD estimation methods [6].

B. Combining data segments

By combining large numbers of time-series data segments it is sometimes possible to extract weak signals not visible in individual segments, for example, to measure the population of gravitational waves from unresolved compact binaries [18, 27–29] and to detect gravitational-wave memory [30]. Combining data segments can also have the effect of magnifying systematic errors that are small enough to ignore when considering just a single segment in isolation. For example, failing to take into account uncertainty in estimates of the noise PSD leads to low-level excess power, which can be mistaken for a population of sub-threshold gravitational-wave signals [6, 25].

Here, we show that the correlations between neighboring frequency bins induced by all windows must be taken into account to avoid systematic error in studies that rely on precision measurements combining many segments. We illustrate this point using simulated data to carry out a mock search for a population of sub-threshold Gaussian bursts in simulated Gaussian noise with a known PSD. We employ the formalism from [18] to estimate the fraction of $M = 160000$ data segments of which 1500 contain a simulated signal.

Our likelihood is a mixture model, which allows for

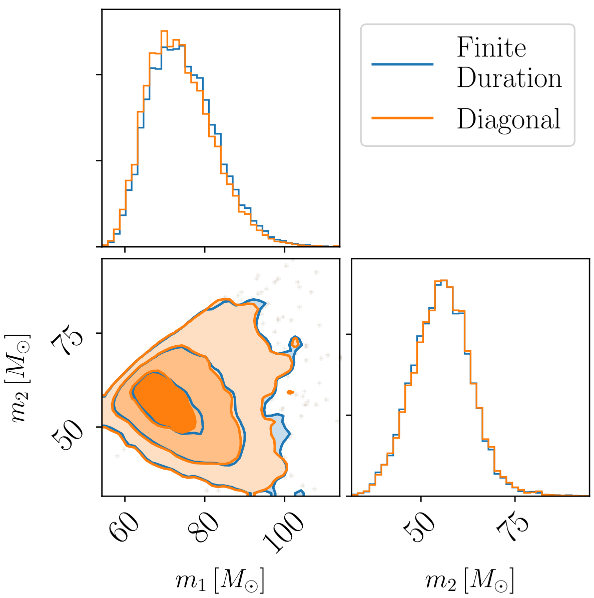

FIG. 7. Intrinsic parameters for the binary black hole merger GW190521 [10] using the diagonal likelihood (blue) and our new finite-duration likelihood (orange). The primary and secondary mass (m_1, m_2) refer respectively to the more-massive and less-massive component masses. Including covariance between neighbouring bins has no observable impact on the inferred posterior.

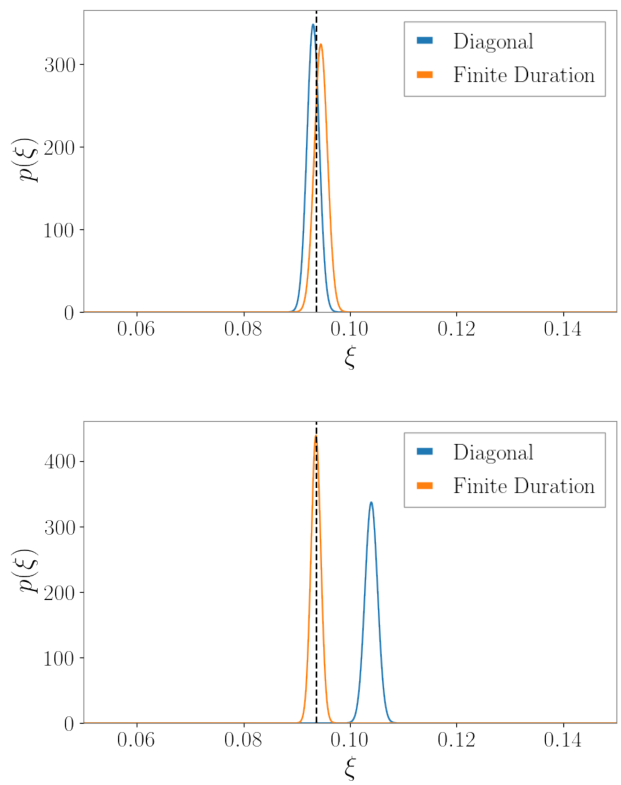

FIG. 8. The posterior distribution for the fraction of segments containing a signal in our toy example (Section III B). We analyze ~ 7.5 days of simulated Gaussian noise divided into $4s$ segments (160000 segments), 15000 of these segments contain a Gaussian pulse with frequency 50 Hz (top) or 500 Hz (bottom). In blue we show the posterior distribution obtained using the standard likelihood that ignores correlations between neighboring frequency bins induced by the window function. In orange, we show the posterior distribution using a likelihood that accounts for these correlations. We see that the diagonal method gives a biased result when the signal is centered at 500 Hz. This is the location of several large spectral lines which increase the importance of correlations between frequencies. We note that when the signal is isolated away from large spectral lines the difference is much more modest.

each segment to consist of either of signal $\mathcal{S}$ or noise $\mathcal{N}$:

$$\mathcal{L}(\{d\}|\xi) = \prod_i^M \Big[\xi\mathcal{L}(d_i|\mathcal{S}) + (1-\xi)\mathcal{L}(d_i|\mathcal{N})\Big]. \tag{28}$$

Here, $\mathcal{L}(d_i|\mathcal{S})$ is the likelihood of data segment i given the signal hypothesis while $\mathcal{L}(d_i|\mathcal{N})$ is the likelihood given the noise hypothesis and the parameter ξ is the fraction of segments that contain a signal. We simulate data in 128 s chunks and break up the data into 4 s segments. We compute the finite duration PSD matrix using the known PSD used to simulate the data. The known PSD is as estimated for the LIGO Livingston detector in our analysis of GW170814. We do not re-estimate the PSD from the simulated data in order to avoid uncertainty intrinsic to the PSD estimation method.

For the toy example considered here, we use a simplified model for the signal hypothesis. We assume that all signals are a Gaussian burst with fixed parameters. We normalize the signal such that the optimal matched filter SNR $= 4$. Therefore the signal is always the same, and we only consider one template $\bar{h}$ [31]. The signal likelihood is then Eq. 24 with template $\bar{h}$, the noise likelihood is Eq. 24 with no template. To demonstrate the frequency dependence of the correction to the likelihood we consider two signals, one centered at 50 Hz and one at 500 Hz. The latter is deliberately chosen to maximize the impact of correlations between neighboring frequencies near the large spectral lines around 500 Hz.

For each iteration, we calculate the posterior for ξ two ways, once using the standard diagonal likelihood and once using the finite-duration likelihood. The results are shown in Fig. 8 for a tukey window with $\alpha = 0.1$. When the signal is far away from large spectral lines (top) the inferred posteriors are different, but both consistent with the true value at high significance. However, when the signal is next to the spectral lines there is a significant bias when neglecting the correlation between neighboring frequencies.

IV. DISCUSSION

As gravitational-wave astronomy matures, the growing catalog of events enables exciting new science. However, as we probe increasingly higher SNRs, and as we combine larger ensembles of data segments, our analyses are increasingly susceptible to systematic error from approximations in our models and data analysis. Many sources of systematic error in our modeling have been considered in recent years including calibration uncertainty [23, 24], waveform systematics [32–35], and noise estimation [6, 25, 26]. In this work, we examine how correlations between frequency bins are inevitably introduced by windowing in time-domain analysis. We show how these correlations can be modeled using a frequency-domain noise covariance matrix, thereby avoiding bias. By performing a singular value decomposition, we identify that the basis that diagonalizes the covariance matrix is not the Fourier basis as usually assumed, but depends on both the PSD and the choice of window function. We demonstrate that, while the impact of the off-diagonal components in the noise covariance matrix is small for individually resolved events, they are important for precision estimates of the Bayesian evidence, especially when the signal overlaps with large spectral lines.

A natural extension of the framework provided here is to incorporate marginalization over sources of systematic uncertainty. Marginalization over waveform or detector calibration uncertainty can be trivially combined with this method. Marginalizing over uncertainty in the PSD estimate would require either modifying the `BayesLine` algorithm [36] to include modeling the full noise covariance matrix or an analytic method such as in [3, 6, 37]. Even after considering all these forms of systematic uncertainty, we still need to develop methods to deal with the non-Gaussianity and non-stationarity of real data. This is an active area of development [38–40]; however, establishing a unified treatment is left to future studies.

ACKNOWLEDGEMENTS

We are grateful to Sharan Banagiri, Katerina Chatziiaonnou, Joe Romano, and Alan Weinstein for many fruitful discussions. CT acknowledges the support of the National Science Foundation, and the LIGO Laboratory. This work is supported through the Australian Research Council (ARC) Centre of Excellence CE170100004. SB is also supported by the Paul and Daisy Soros Fellowship for New Americans, the Australian-American Fulbright Commission, and the NSF Graduate Research Fellowship under Grant No. DGE-1122374. This research has made use of data, software, and/or web tools obtained from the Gravitational Wave Open Science Center [41, 42] (https://www.gw-openscience.org), a service of LIGO Laboratory, the LIGO Scientific Collaboration and the Virgo Collaboration. LIGO is funded by the U.S. National Science Foundation. Virgo is funded by the French Centre National de Recherche Scientifique (CNRS), the Italian Istituto Nazionale della Fisica Nucleare (INFN), and the Dutch Nikhef, with contributions by Polish and Hungarian institutes. The authors are grateful for computational resources provided by the LIGO Lab and supported by National Science Foundation Grants PHY-0757058 and PHY-0823459. This is document LIGO-P2100090.

`Cython` and `CUDA` implementations and `Python` wrappers of the PSD matrix calculation are available at github.com/ColmTalbot/psd-covariance-matrices.

Appendix A: Connection to coarse-grained PSD estimation

While time-averaging of short segments to estimate power spectral densities (e.g., Welch averaging) is common in gravitational-wave data analysis, an alternative "coarse-graining" method is used in some areas, especially searches for the stochastic gravitational-wave background; see, e.g., [14]. In this appendix, we demonstrate that coarse-graining is a special case of the projection method we use in this work.

The coarse-grained PSD is defined for a frequency resolution δf as

$$S_i = \frac{1}{\delta f} \int_{f_i - \delta f/2}^{f_i + \delta f/2} df \mathcal{S}(f) \tag{A1}$$

$$= \frac{1}{\delta f} \int_{-\infty}^{\infty} df \Pi(f_i - \delta f/2, f_i + \delta f/2) \mathcal{S}(f) \tag{A2}$$

$$= \frac{1}{\alpha} \mathcal{S}_\mu |\tilde{w}_{\mu - \alpha i}|^2 \quad \alpha \in \mathbb{Z} \tag{A3}$$

$$\tilde{w}_\mu = \begin{cases} 1 & -\frac{\alpha}{2} < \mu < \frac{\alpha}{2} \\ 0.5 & |\mu| = \frac{\alpha}{2} \quad \text{if } \frac{\alpha}{2} \in \mathbb{Z} \\ 0 & \text{else} \end{cases} \tag{A4}$$

In the second line, Π is the unit boxcar function. As for the window operator in this work, we can express this as a circulant matrix with non-zero entries only in a small region. The corresponding time-domain window is the sinc function. We note that the coarsened frequency-domain covariance matrix is diagonal by construction in this case.

Appendix B: Computing the finite-duration covariance matrix

For a typical 4 s data segment, with sampling frequency 2048 Hz, analyzed with a 1/128 Hz noise model, we must perform the matrix operations in Equation 16 with $\mathcal{O}(2^{18} \times 2^{18})$ elements. A naive implementation at double precision would require a prohibitive amount of computational resources. Fortunately, the computation can be performed much more computationally efficiently. The first thing we note is that $\mathcal{C}_{\mu\nu}$ is diagonal and $\tilde{W}_{\mu\nu}$

is a circulant matrix, i.e., it is fully specified by a single row/column ($\tilde{w}_\mu$). Since each matrix can be represented using a single vector, we do not need to form any matrices with the 1/128 Hz resolution, dramatically reducing memory requirements. We also identify that C_{ij} is a Hermitian matrix, reducing the computational cost by a factor of two.

We provide functions to compute the coarsened PSD matrix from a frequency-domain window and PSD implemented in `Cython` and `cupy` compatible `CUDA`. The former runs in $\mathcal{O}(N^3)$ time and the latter in $\mathcal{O}(N)$ wall time. The latter is used to produce the results in this paper and is less computationally expensive than the SVD performed on the coarsened data.

In Algorithm 1, we describe the process used to compute the regularized inverse covariance matrices used for our binary black hole anlayses.

Appendix C: Additional figures

In this Appendix we show the PSD matrix (top left), regularized PSD matrix (top right), SVD eigenmatrix (bottom left), and regularized inverse PSD matrix (bottom right) for our analysis of GW170814 for LIGO Hanford (Fig. 9), LIGO Livingston (Fig. 10), and Virgo (Fig. 11). We note that the data for all three interferometers show the same qualitative features and quantitative differences determined by the specific sensitivity of each interferometer.

We see that the PSD matrix is dominated by the leading diagonal and nearby frequencies and correlations at frequencies corresponding to spectral lines. The correlations from the spectral lines are less pronounced in the regularized PSD matrix, however, there is more broadband correlation between frequencies above/below the most sensitive frequency. The divide between frequencies above and below the most sensitive frequency can also be seen in the SVD and regluarized inverse PSD matrices.

[1] Fredric J. Harris, "On the Use of Windows for Harmonic Analysis with the Discrete Fourier Transform," IEEE Proceedings **66**, 51–83 (1978).

[2] Nidhan Choudhuri, Subhashis Ghosal, and Anindya Roy, "Contiguity of the Whittle measure for a Gaussian time series," Biometrika **91**, 211–218 (2004), https://academic.oup.com/biomet/article-pdf/91/1/211/582804/910211.pdf.

[3] Christian Röver, "Student-t based filter for robust signal detection," Phys. Rev. D **84**, 122004 (2011), arXiv:1109.0442.

[4] Adam M. Sykulski, Sofia C. Olhede, Arthur P. Guillaumin, Jonathan M. Lilly, and Jeffrey J. Early, "The De-Biased Whittle Likelihood," (2016), arXiv:1605.06718 [stat.ME].

[5] Claudia Kirch, Matthew C. Edwards, Alexander Meier, and Renate Meyer, "Beyond Whittle: Nonparametric correction of a parametric likelihood with a focus on Bayesian time series analysis," (2017), arXiv:1701.04846 [stat.ME].

[6] Colm Talbot and Eric Thrane, "Gravitational-wave astronomy with an uncertain noise power spectral density," Physical Review Research **2**, 043298 (2020), arXiv:2006.05292 [astro-ph.IM].

[7] "A simple introduction to the klt (karhunen—loève transform)," in *Deep Space Flight and Communications: Exploiting the Sun as a Gravitational Lens* (Springer Berlin Heidelberg, Berlin, Heidelberg, 2009) pp. 151–179.

[8] B. P. Abbott *et al.*, "Observation of Gravitational Waves from a Binary Black Hole Merger," Phys. Rev. Lett. **116**, 061102 (2016), arXiv:1602.03837 [gr-qc].

[9] B. P. Abbott *et al.*, "GW170814: A Three-Detector Observation of Gravitational Waves from a Binary Black Hole Coalescence," Phys. Rev. Lett. **119**, 141101 (2017), arXiv:1709.09660 [gr-qc].

[10] R. Abbott *et al.*, "GW190521: A Binary Black Hole Merger with a Total Mass of 150 $M_\odot$," Phys. Rev. Lett. **125**, 101102 (2020), arXiv:2009.01075 [gr-qc].

[11] J. Aasi *et al.*, "Advanced LIGO," Classical and Quantum Gravity **32**, 074001 (2015), arXiv:1411.4547 [gr-qc].

[12] F. Acernese *et al.*, "Advanced Virgo: a second-generation interferometric gravitational wave detector," Classical and Quantum Gravity **32**, 024001 (2015), arXiv:1408.3978 [gr-qc].

[13] We note that here we use two-sided discrete Fourier transforms rather than the one-sided version widely used in gravitational-wave data analysis.

[14] J. Aasi *et al.*, "Improved Upper Limits on the Stochastic Gravitational-Wave Background from 2009-2010 LIGO and Virgo Data," Phys. Rev. Lett. **113**, 231101 (2014), arXiv:1406.4556 [gr-qc].

[15] P. B. Covas, A. Effler, E. Goetz, P. M. Meyers, A. Neunzert, M. Oliver, B. L. Pearlstone, V. J. Roma, R. M. S. Schofield, V. B. Adya, *et al.*, "Identification and mitigation of narrow spectral artifacts that degrade searches for persistent gravitational waves in the first two observing runs of Advanced LIGO," Phys. Rev. D **97**, 082002 (2018), arXiv:1801.07204 [astro-ph.IM].

[16] The covariance matrix is non-invertible as the window application is not reversible. There is no way to recover the value of the time series for points at which the data have been zeroed, e.g., the end points.).

[17] Eric Thrane and Colm Talbot, "An introduction to Bayesian inference in gravitational-wave astronomy: Parameter estimation, model selection, and hierarchical models," Pub. Astron. Soc. Aust. **36**, e010 (2019), arXiv:1809.02293 [astro-ph.IM].

[18] Rory Smith and Eric Thrane, "Optimal Search for an

Algorithm 1: Computing the regularized inverse PSD matrix from real data

Result: regularized inverse PSD matrix (Equation 21)
load $512s$ of data ending $2s$ before the analysis segment begins;
divide into 4 $128s$ chunks;
apply a Hann window (Tukey $\alpha = 1$) to each chunk and FFT;
take a median average of power in each chunk to generate the "infinite"-duration PSD ($\mathcal{S}_\mu$);
define the infinite-duration window (w_ψ) as a $128s$ time series according to Equation 12;
compute the finite-duration covariance matrix (C_{ij}) using Equation 16;
compute the SVD (Equation 18) and regularized inverse ($\bar{C}_{ij}$) as outlined in Section II E;

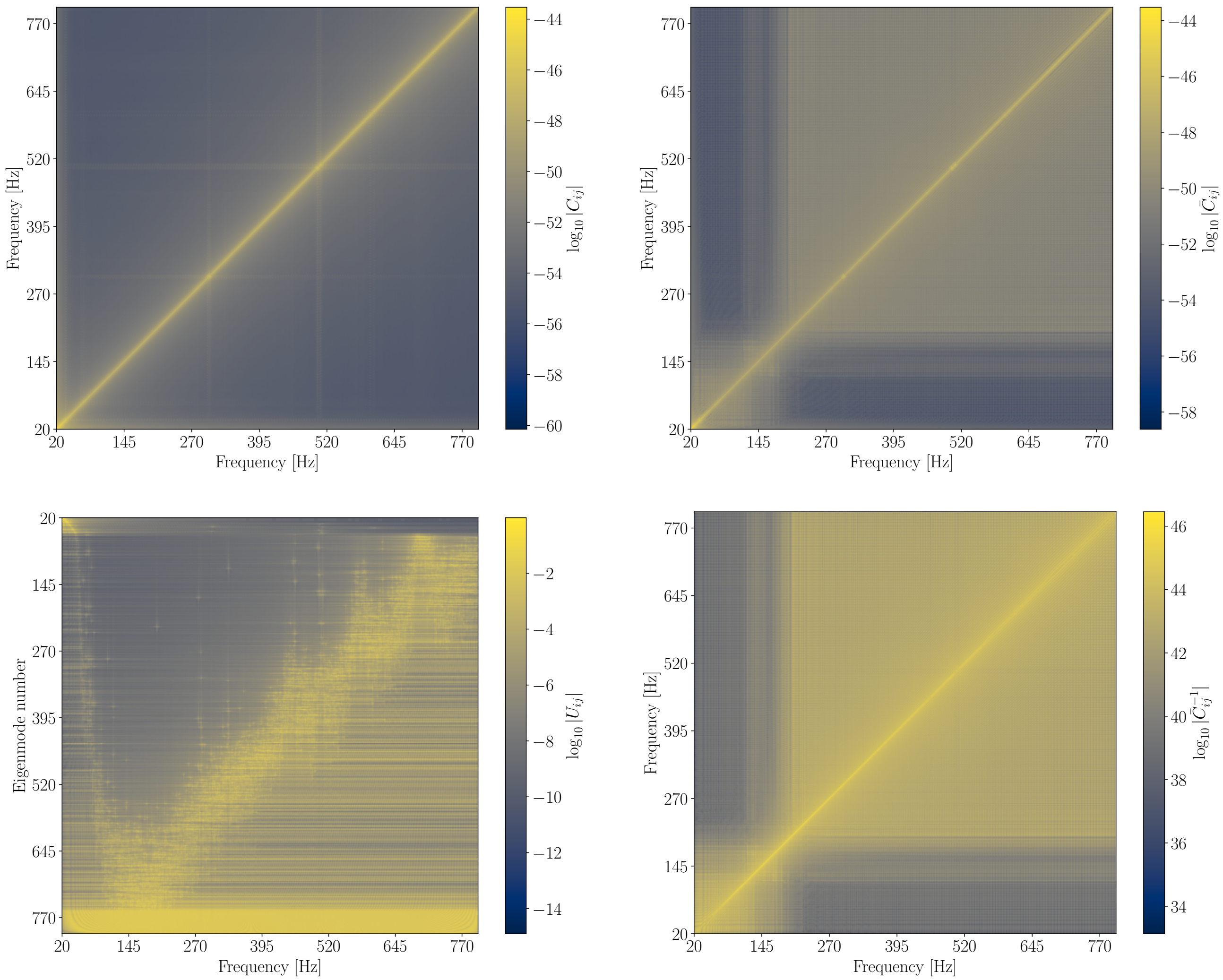

FIG. 9. PSD matrix (top left), regularized PSD matrix (top right), SVD eigenmatrix (bottom left), and regularized inverse PSD matrix (bottom right) for the LIGO Hanford observatory at the time of GW170814.

Astrophysical Gravitational-Wave Background," Physical Review X **8**, 021019 (2018), arXiv:1712.00688 [gr-qc].
[19] Duncan Macleod, Alex L. Urban, Scott Coughlin, Thomas Massinger, Matt Pitkin, rngeorge, paulaltin, Joseph Areeda, Leo Singer, Eric Quintero, Katrin Leinweber, and The Gitter Badger, "gwpy/gwpy: 2.0.4," (2021).
[20] Geraint Pratten, Sascha Husa, Cecilio Garcia-Quiros, Marta Colleoni, Antoni Ramos-Buades, Hector Estelles, and Rafel Jaume, "Setting the cornerstone for a family of models for gravitational waves from compact binaries: The dominant harmonic for nonprecessing quasi-circular black holes," Phys. Rev. D **102**, 064001 (2020), arXiv:2001.11412 [gr-qc].
[21] Cecilio García-Quirós, Marta Colleoni, Sascha Husa, Héctor Estellés, Geraint Pratten, Antoni Ramos-Buades, Maite Mateu-Lucena, and Rafel Jaume, "Multimode frequency-domain model for the gravitational wave sig-

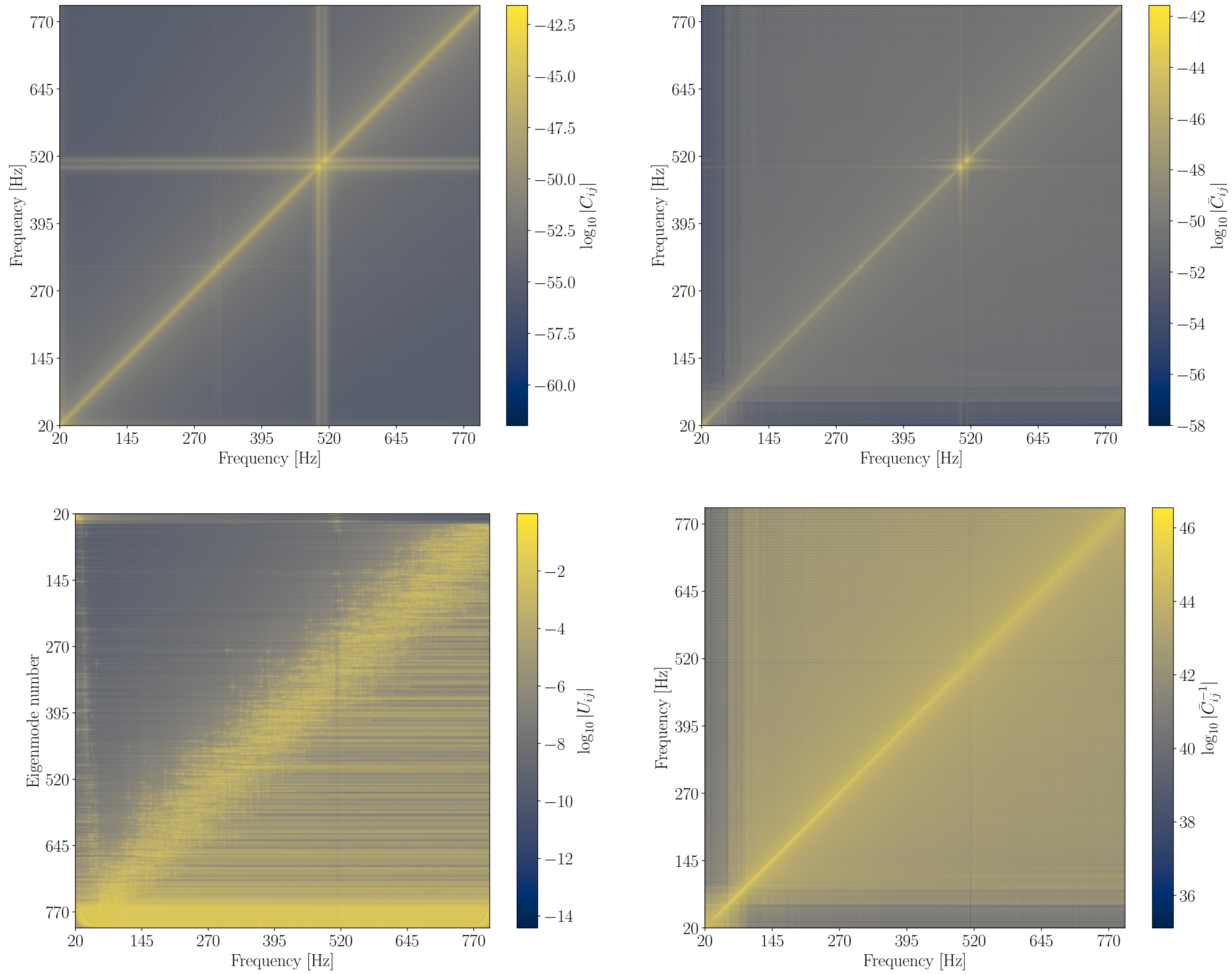

FIG. 10. PSD matrix (top left), regularized PSD matrix (top right), SVD eigenmatrix (bottom left), and regularized inverse PSD matrix (bottom right) for the LIGO Livingston observatory at the time of GW170814.

nal from nonprecessing black-hole binaries," Phys. Rev. D **102**, 064002 (2020), arXiv:2001.10914 [gr-qc].

[22] Geraint Pratten, Cecilio García-Quirós, Marta Colleoni, Antoni Ramos-Buades, Héctor Estellés, Maite Mateu-Lucena, Rafel Jaume, Maria Haney, David Keitel, Jonathan E. Thompson, and Sascha Husa, "Computationally efficient models for the dominant and subdominant harmonic modes of precessing binary black holes," Phys. Rev. D **103**, 104056 (2021), arXiv:2004.06503 [gr-qc].

[23] Ethan Payne, Colm Talbot, Paul D. Lasky, Eric Thrane, and Jeffrey S. Kissel, "Gravitational-wave astronomy with a physical calibration model," Phys. Rev. D **102**, 122004 (2020), arXiv:2009.10193 [astro-ph.IM].

[24] Salvatore Vitale, Carl-Johan Haster, Ling Sun, Ben Farr, Evan Goetz, Jeff Kissel, and Craig Cahillane, "Physical approach to the marginalization of LIGO calibration uncertainties," Phys. Rev. D **103**, 063016 (2021), arXiv:2009.10192 [gr-qc].

[25] Sylvia Biscoveanu, Carl-Johan Haster, Salvatore Vitale, and Jonathan Davies, "Quantifying the effect of power spectral density uncertainty on gravitational-wave parameter estimation for compact binary sources," Phys. Rev. D **102**, 023008 (2020), arXiv:2004.05149 [astro-ph.HE].

[26] Katerina Chatziioannou, Carl-Johan Haster, Tyson B. Littenberg, Will M. Farr, Sudarshan Ghonge, Margaret Millhouse, James A. Clark, and Neil Cornish, "Noise spectral estimation methods and their impact on gravitational wave measurement of compact binary mergers," Phys. Rev. D **100**, 104004 (2019), arXiv:1907.06540 [gr-qc].

[27] Sebastian M. Gaebel, John Veitch, Thomas Dent, and Will M. Farr, "Digging the population of compact binary mergers out of the noise," Mon. Not. R. Ast. Soc. **484**, 4008–4023 (2019), arXiv:1809.03815 [astro-ph.IM].

[28] Rory J. E. Smith, Colm Talbot, Francisco Hernandez Vivanco, and Eric Thrane, "Inferring the population properties of binary black holes from unresolved gravitational waves," Mon. Not. R. Ast. Soc. **496**, 3281–3290 (2020),

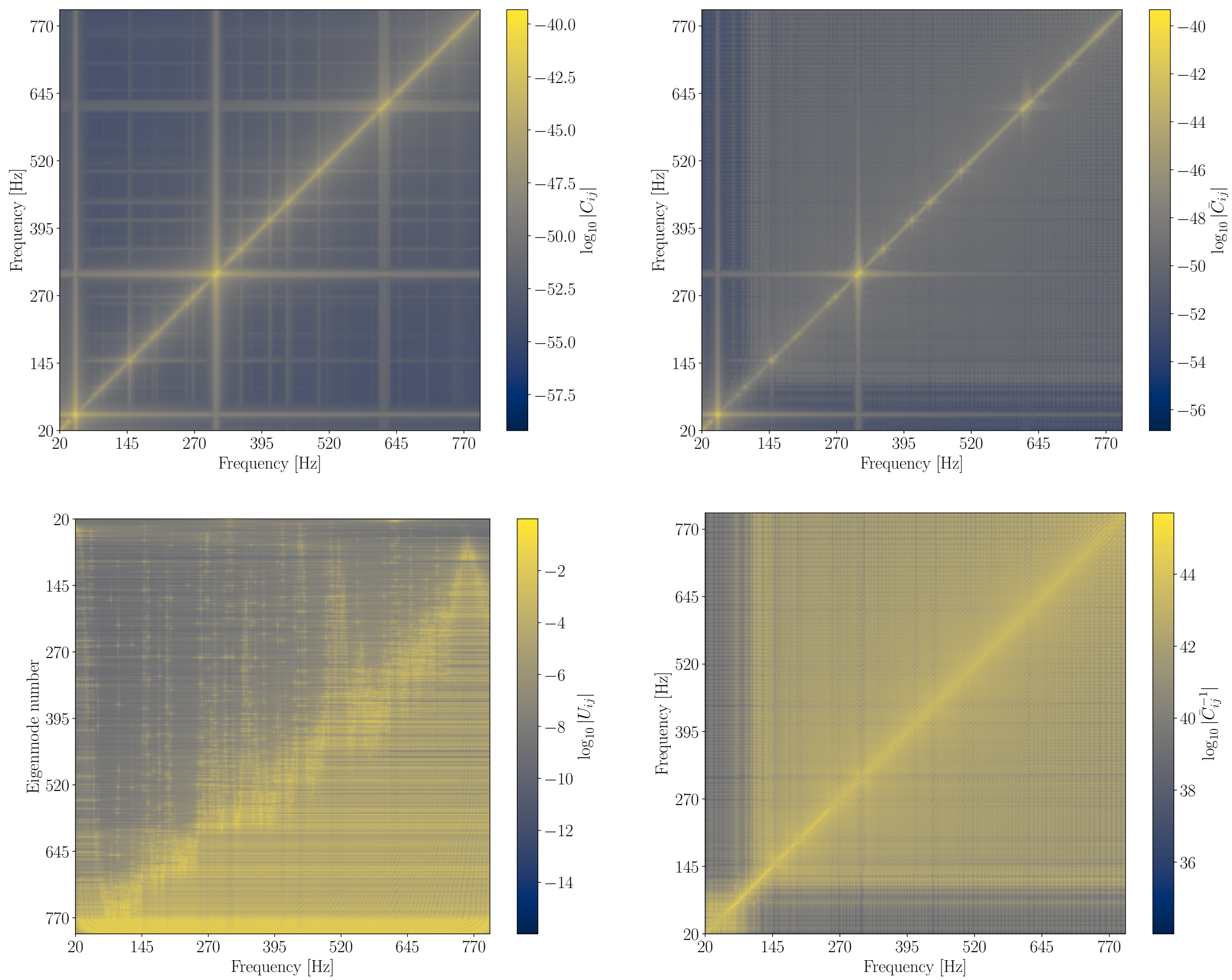

FIG. 11. PSD matrix (top left), regularized PSD matrix (top right), SVD eigenmatrix (bottom left), and regularized inverse PSD matrix (bottom right) for the Virgo observatory at the time of GW170814.

arXiv:2004.09700 [astro-ph.HE].

[29] Sharan Banagiri, Vuk Mandic, Claudia Scarlata, and Kate Z. Yang, "Measuring angular N -point correlations of binary black hole merger gravitational-wave events with hierarchical Bayesian inference," Phys. Rev. D **102**, 063007 (2020), arXiv:2006.00633 [astro-ph.CO].

[30] Paul D. Lasky, Eric Thrane, Yuri Levin, Jonathan Blackman, and Yanbei Chen, "Detecting Gravitational-Wave Memory with LIGO: Implications of GW150914," Phys. Rev. Lett. **117**, 061102 (2016), arXiv:1605.01415 [astro-ph.HE].

[31] We emphasize that this method trivially extends to the more generic case of an unknown population of signals, however, we make this assumption to isolate the impact of the covariance matrix.

[32] Gregory Ashton and Sebastian Khan, "Multiwaveform inference of gravitational waves," Phys. Rev. D **101**, 064037 (2020), arXiv:1910.09138 [gr-qc].

[33] Michael Pürrer and Carl-Johan Haster, "Gravitational waveform accuracy requirements for future ground-based detectors," Physical Review Research **2**, 023151 (2020), arXiv:1912.10055 [gr-qc].

[34] A. Z. Jan, A. B. Yelikar, J. Lange, and R. O'Shaughnessy, "Assessing and marginalizing over compact binary coalescence waveform systematics with RIFT," Phys. Rev. D **102**, 124069 (2020), arXiv:2011.03571 [gr-qc].

[35] Héctor Estellés, Sascha Husa, Marta Colleoni, Maite Mateu-Lucena, Maria de Lluc Planas, Cecilio García-Quirós, David Keitel, Antoni Ramos-Buades, Ajit Kumar Mehta, Alessandra Buonanno, and Serguei Ossokine, "A detailed analysis of GW190521 with phenomenological waveform models," arXiv e-prints , arXiv:2105.06360 (2021), arXiv:2105.06360 [gr-qc].

[36] Tyson B. Littenberg and Neil J. Cornish, "Bayesian inference for spectral estimation of gravitational wave detector noise," Phys. Rev. D **91**, 084034 (2015), arXiv:1410.3852 [gr-qc].

[37] Sharan Banagiri, Michael W. Coughlin, James Clark, Paul D. Lasky, M. A. Bizouard, Colm Talbot,

Eric Thrane, and Vuk Mandic, "Constraining the gravitational-wave afterglow from a binary neutron star coalescence," Mon. Not. R. Ast. Soc. **492**, 4945–4951 (2020), arXiv:1909.01934 [astro-ph.IM].

[38] Barak Zackay, Tejaswi Venumadhav, Javier Roulet, Liang Dai, and Matias Zaldarriaga, "Detecting Gravitational Waves in Data with Non-Gaussian Noise," (2019), arXiv:1908.05644 [astro-ph.IM].

[39] Neil J. Cornish, "Time-frequency analysis of gravitational wave data," Phys. Rev. D **102**, 124038 (2020), arXiv:2009.00043 [gr-qc].

[40] O Edy, A. Lundgren, and L. K. Nuttall, "The Issues of Mismodelling Gravitational-Wave Data for Parameter Estimation," (2021), arXiv:2101.07743 [astro-ph.IM].

[41] Michele Vallisneri, Jonah Kanner, Roy Williams, Alan Weinstein, and Branson Stephens, "The LIGO Open Science Center," J. Phys. Conf. Ser. **610**, 012021 (2015), arXiv:1410.4839.

[42] The LIGO Scientific Collaboration, R. the Virgo Collaboration and Abbott, *et al.*, "Open data from the first and second observing runs of Advanced LIGO and Advanced Virgo," (2019), arXiv:1912.11716 [gr-qc].